GSA Data Repository 2014261

Explosive to effusive transition during the largest volcanic eruption of the 20th century (Novarupta 1912, Alaska)

Chinh T. Nguyen[1]*, Helge M. Gonnermann[1], Bruce F. Houghton[2]

[1]Department of Earth Science, Rice University, Houston, Texas, 77005, USA.

[2]Department of Geology and Geophysics, University of Hawai'i at Manoa, Honolulu, HI 96822, USA.

*E-mail: ctn2@rice.edu.

POROSITY MEASUREMENTS

Samples were cored into cylinders of 1 cm diameter and 1-5 cm length. Pycnometry was performed using a Micromeritics AccuPyc II 1340©, which determined the skeletal sample volume, V_{ske} (the sum of the volumes of both solid and isolated pores), by measuring the pressure change of helium within the calibrated volume and using Boyle's law. Then the volume of connected pores was calculated as $V_{con} = V_{sample} - V_{ske}$, where V_{sample} is the volume of cylindrical core of the sample. Powderized samples were also measured using the AccuPyc II 1340© to determine the density of the skeleton (solid plus any isolated vesicles that not somehow connected to the sample surface), which then was used to calculate the volume of isolated pores, V_{iso}. Finally, connected and total porosity were calculated as $\phi_{con} = V_{con} / V_{sample}$, and $\phi_{total} = (V_{con} + V_{iso}) / V_{sample}$. Measured porosity values of all samples are listed in Table DR1.

Table DR1. Porosity and permeability of all samples from five episodes of Novarupta 1912 eruption.

	Sample ID	ϕ_{con}(%)	ϕ_{total}(%)	k_1(m^2)	k_2(m)
Episode I (Plinian)	89 – 1 – 5 – 1 – 2	65.46	77.81	2.63 x 10^{-14}	6.63 x 10^{-11}
	89 – 1 – 5 – 2 – 1	56.01	76.02	7.47 x 10^{-14}	1.44 x 10^{-10}
	89 – 1 – 5 – 2 – 2 – 1	58.02	76.86	3.11 x 10^{-13}	4.90 x 10^{-10}
	89 – 1 – 5 – 5 – 2	45.46	69.28	4.13 x 10^{-14}	1.68 x 10^{-10}
	89 – 1 – 5 – 6 – 1	63.54	77.76	4.21 x 10^{-13}	1.65 x 10^{-9}
	89 – 1 – 5 – 6 – 2	59.41	75.60	9.87 x 10^{-13}	5.81 x 10^{-9}
	89 – 1 – 5 – 9	63.21	78.69	4.45 x 10^{-14}	1.44 x 10^{-10}
	89 – 1 – 5 – 21	70.28	82.36	5.17 x 10^{-14}	9.18 x 10^{-11}
	89 – 1 – 5 – 27	49.50	68.35	1.82 x 10^{-15}	2.36 x 10^{-10}
	89 – 1 – 12 – 3	66.68	75.62	2.16 x 10^{-12}	3.64 x 10^{-9}
	89 – 1 – 12 – 4 – 2	63.81	73.65	3.65 x 10^{-15}	9.76 x 10^{-12}
	89 – 1 – 12 – 6	63.65	73.05	1.24 x 10^{-14}	2.04 x 10^{-11}
	89 – 1 – 12 – 7 – 1	72.48	84.31	1.44 x 10^{-13}	2.72 x 10^{-10}
	89 – 1 – 12 – 7 – 2	70.05	83.21	4.52 x 10^{-14}	1.30 x 10^{-10}

Episode II (Plinian)	94 – 01 – 11 – 02	70.77	75.30	1.28×10^{-13}	4.05×10^{-10}
	94 – 01 – 11 – 03	71.07	75.17	2.16×10^{-14}	2.70×10^{-11}
	94 – 01 – 11 – 04	81.97	84.19	9.41×10^{-14}	4.31×10^{-10}
	94 – 01 – 11 – 05	72.99	77.84	2.50×10^{-13}	4.96×10^{-10}
Episode III (Plinian)	94 – 01 – 2003 – 17 – 1	60.41	65.20	1.82×10^{-13}	7.24×10^{-10}
	94 – 01 – 2003 – 17 – 2	81.11	84.15	8.88×10^{-13}	5.01×10^{-9}
	94 – 01 – 2003 – 17 – 3	68.86	74.51	4.18×10^{-12}	1.40×10^{-7}
	94 – 01 – 2003 – 17 – 4	69.58	76.49	4.34×10^{-14}	6.20×10^{-10}
	94 – 01 – 2003 – 17 – 14	59.59	66.44	1.26×10^{-14}	3.27×10^{-11}
	94 – 01 – 2D – 01	62.02	74.09	9.98×10^{-13}	7.67×10^{-9}
	94 – 01 – 2D – 02	61.41	62.54	3.06×10^{-13}	9.81×10^{-10}
	94 – 01 – 2D – 03	62.32	69.51	2.20×10^{-12}	8.40×10^{-8}
	94 – 01 – 2D – 04	65.36	70.18	4.87×10^{-13}	2.05×10^{-9}
	94 – 01 – 7D – 01	64.90	74.59	2.16×10^{-12}	9.86×10^{-8}
	94 – 01 – 7D – 02	63.22	74.34	2.34×10^{-12}	3.97×10^{-7}
Episode IV (Pumiceous)	Post – H – Blocks – 7	53.07	62.34	4.06×10^{-14}	9.21×10^{-11}
	Post – H – Blocks – 9	54.21	59.31	5.42×10^{-15}	1.44×10^{-11}
	Post – H – Blocks – 15 – 2	74.22	78.80	2.10×10^{-12}	1.92×10^{-8}
	Post – H – Blocks – 17 – 1	56.51	62.36	1.35×10^{-13}	2.94×10^{-10}
	Post – H – Blocks – 22	65.65	71.84	3.68×10^{-13}	2.29×10^{-9}
	Post – H – Blocks – 24	71.67	76.67	3.83×10^{-12}	1.28×10^{-7}
	Post – H – Blocks – 43	61.30	67.78	1.07×10^{-13}	3.57×10^{-10}
Episode V (Dome)	R – Dome – 5 – 1	34.97	46.63	3.78×10^{-15}	5.25×10^{-12}
	R – Dome – 5 – 2	37.67	48.60	1.98×10^{-14}	6.50×10^{-11}
	R – Dome – 8 – 2	28.70	41.98	5.28×10^{-16}	7.57×10^{-14}
	R – Dome – 10	23.64	36.28	1.97×10^{-16}	6.13×10^{-15}
	R – Dome – 15	17.44	29.86	1.62×10^{-15}	1.41×10^{-12}
	R – Dome – 22 – 1	19.90	30.57	1.11×10^{-15}	5.63×10^{-13}
	R – Dome – 22 – 2	16.90	29.23	2.48×10^{-16}	3.21×10^{-14}
	R – Dome – 32	43.33	54.00	2.31×10^{-13}	2.33×10^{-9}

PERMEABILITY MEASUREMENTS

Permeability was measured using Capillary Flow Porometer (Model CFP-1100AXL-AC, Porous Media, Inc. ©). Samples were sealed with impermeable epoxy resin and then mounted on plexi-glass plates for permeability measurements. These samples were then placed in a chamber and completely sealed except at the two ends. At the inlet air pressure, P_{in}, varied from 1.1×10^5 Pa up to 6×10^5 Pa; whereas the outlet pressure, P_{out}, at the other end was at atmospheric pressure. Each sample was measured using 2-3 interchangeable flow meters, in order to achieve several orders of magnitude in flow rates at optimal accuracy. For all measurements, the controlled pressure gradient across the sample length was thus between 0 and 5×10^5 Pa m^{-1}, and the measured volumetric flow rate of air, Q, was between 3×10^{-3} and 5×10^{-7} m^3 s^{-1}, with an accuracy ~ 5×10^{-8} m^3 s^{-1} (~ 1% of the minimum measured flow rate). After the measurements, samples were sectioned and examined under a transmitted light microscope, as well as a scanning electron microscope for cracks. Only samples that showed no cracks of any size are reported.

PERMEABILITY ESTIMATION

We estimate permeability using Forchheimer's equation (Reynolds, 1901; Forchheimer, 1900; Rust and Cashman, 2004) for a compressible gas as follows,

$$\frac{P_{in}^2 - P_{out}^2}{2PL} = \frac{\mu}{k_1}\frac{Q}{A} + \frac{\rho}{k_2}\left(\frac{Q}{A}\right)^2, \qquad (1)$$

where P is the pressure at which flow rate is measured, that is $P = P_{out} = 1$ atmosphere. Furthermore, $\mu = 1.86\text{x}10^{-5}$ Pa s is the air viscosity, $\rho = 1.28$ kg m^{-3} is the air density, A is the cross-sectional area of the sample, k_1 is the Darcian permeability and k_2 is known as the inertial permeability.

Due to the turbulent viscous dissipation flow curves become parabolic (Fig. 1a), instead of linear, at high values of Q. This turbulent dissipation is accounted for by the k_2 term of Eq. (1) when fitting the Q vs. $\Delta P = P_{in} - P_{out}$ data (i.e., the flow curves). In order to determine the combination of k_1 and k_2, we calculated the root-mean-square error between measured values of $Q(\Delta P)$ and those predicted by Eq. (1) for systematically different combinations of k_1 and k_2. In other words, we use a grid search to find the values of k_1 and k_2 that minimize the root-mean-square error, defined as

$$\chi = \left[\frac{1}{N}\sum_{1}^{N}\left(1 - \frac{Q_{predicted}}{Q_{measured}}\right)^2\right]^{1/2}, \qquad (2)$$

where N is the number of data points for a given sample. A typical example of such grid search is shown in Fig. DR1. This result is typical of all our data and illustrates that the flow curves are indeed well fitted by Eq. (1). The relationship between k_1 and k_2 for all of our samples is shown in Fig. (2) and similar to what has been reported elsewhere (e.g., Rust and Cashman, 2004). Permeability values of all samples are listed in Table DR1.

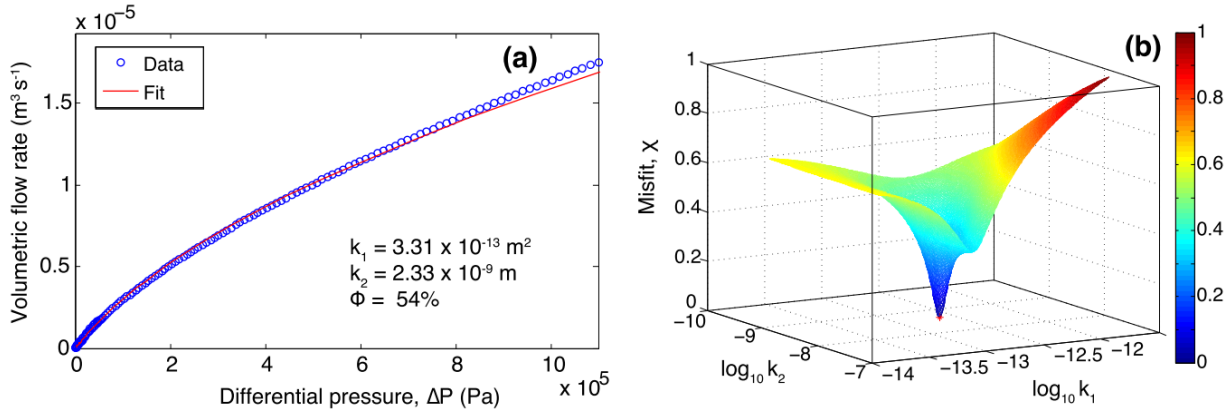

Figure DR1. Illustrative example of permeability estimation. (a) Measured volumetric flow rate (blue circles) as a function of pressure difference across sample, obtained using two different flow meters (100 cm^3 min^{-1} and 1000 cm^3 min^{-1}), and the best fit to the data (red curve).

(b) Misfit χ as a function of $\log_{10}(k_1)$ and $\log_{10}(k_2)$. The combination of k_1 and k_2 that gives the best fit shown as the red star.

NUMERICAL MODELING

We performed numerical modeling of magma ascent coupled with diffusive bubble growth for both H_2O and CO_2. The change in ambient pressure with depth is calculated from the momentum and mass balance of magma flow within the conduit. The conduit flow calculations depend on viscosity of the magma, which in turn depends on the dissolved H_2O within the melt and the volume fraction of bubbles, both of which are calculated from diffusive bubble growth. Diffusive bubble growth in turn depends on the change in ambient pressure, which thereby couples diffusive bubble growth with conduit flow.

Modeling was for the sustained explosive Episodes I-III, as well as a case equivalent to Episodes II and III, but at a lower discharge rate, in order to illustrate the effect of lower discharge rate on eruption dynamics. Discharge rates were based on estimates published in Hildreth and Fierstein (2012) and details of the model parameters are listed in Tables 2 and 3.

Table DR2. Compositions of Novarupta samples[a] and parameters used for modeling[b]

Sample	SiO_2 matrix glass wt.%	wt.% phenocryst	vol.% rhyolite[c]	vol.% dacite[c,d]	vol.% andesite[c]	Ave. mass discharge rate (kg s^{-1})
Episode I (A)	78.8	1-5	100	0	0	$5x10^8$
Episode I (B)	72.9-78.7	1-42	47	27	26	$5x10^8$
Episode II	76.6	25-42	0	100	0	$1.6x10^8$
Episode III	76.6	25-42	6	94	0	$1.1x10^8$
Episode IV	76.6	25-42	N/A	N/A	N/A	N/A
Episode V	78.1	1-5	>95	<5	<1	N/A

[a] Hildreth and Fierstein (2012) and references therein.
[b] Modeling was limited to Epsiodes I (A), II and III.
[c] Relative volumetric proportion of compositional components erupted during the given episode.
[d] Matrix (melt) is rhyolitic in composition and bulk composition is due to phenocrysts.

Table DR3. Model parameters and values

	Episode I	Episode II	Episode III	Low discharge
Mass discharge[a], Q (kg s^{-1})	$5x10^8$	$1.6x10^8$	$1.1x10^8$	$6x10^5$
Initial pressure[b], p_m (MPa)	100	125	125	125
Vapor saturation[b] (mole fraction CO_2)	0	0.5	0.5	0.5
Volume fraction phenocryst in matrix[a]	0.02	0.4	0.4	0.4
Bubble number density (m^{-3})	10^{14}	10^{14}	10^{14}	10^{14}
Conduit radius, a (m)	100	100	100	100
Percolation threshold, ϕ_c	0.65 (0.5)	0.58	0.55	0.55
Power-law coefficient, *n*	4	3.75	3.5	3.5

[a] Based on Hildreth and Fierstein (2012) and references therein.
[b] Initial pressures and vapor saturation are based on the work of Coombs and Gardner (2001) and Hammer et al. (2002)

Conduit Flow Model

The model assumes steady isothermal flow at a constant discharge rate, Q, within a one-dimensional cylindrical conduit of constant radius, a. The change in ambient pressure p_m is calculated from the equation of momentum balance (e.g., Wilson et al., 1980; Dobran, 1992; Mastin, 2002)

$$\frac{dp_m}{dz} = -\rho g - f_m \frac{\rho u^2}{4a} - \rho u \frac{du}{dz} \ , \qquad (7)$$

together with the equation of mass balance,

$$\frac{d(\rho u)}{dz} = 0 . \qquad (8)$$

Here $\rho = \rho_m (1 - \phi)$ is the magma density; ρ_m is the density of the melt; g is the gravitational acceleration; $u = dz/dt = Q/(\pi a^2 \rho)$ is the magma ascent velocity; $f_m = 64/\mathrm{Re} + f_0$ is the friction factor for pipe flow. $\mathrm{Re} = \rho u a / \eta$ is the Reynolds number, and $f_0 = 0.02$ (e.g., Wilson et al., 1980; Dobran, 1992; Mastin, 2002) .

Magma viscosity, η, is calculated using the viscosity formulation for bubble-bearing liquids (Pal, 2003), with the liquid viscosity given by the composition-, temperature- and dissolved water-dependent viscosity of the melt phase, using the formulation of Hui and Zhang (2007). In addition, the effect of phenocrysts is accounted for using the Krieger-Dougherty equation (e.g., Mader et al., 2013) with a critical packing fraction of 0.65 and an exponent of -2.5 (e.g., Gonnermann and Manga, 2007).

Diffusive Bubble Growth Model

As ambient pressure, p_m, decreases the solubility of H_2O and CO_2 decreases, causing them to diffuse into bubbles. In addition, the density of the exsolved H_2O-CO_2 vapor mixture decreases as pressure decreases. Together, diffusion of H_2O and CO_2 into bubble and decrease in density result in bubble growth, which in turn is resisted by viscosity of the surrounding melt. Therfore, diffusive bubble growth couples the conservation of mass for H_2O and CO_2 with the diffusion of H_2O and CO_2 within the melt and momentum balance for the bubble and surrounding melt.

We use the isothermal formulation first published by Amon and Denson (1984) and Arefmanesh and Advani (1991) and subsequently applied to bubbles in magma by Proussevitch et al. (1993). The approach follows close to that presented in Gonnermann and Houghton (2012).

Assuming that the bubbles exist in a uniform packing geometry, we model one idealized representative bubble of spherical shape, which is surrounded by a melt shell with the thickness of $S - R$, where S is the outer radius and R is the final bubble radius. The momentum balance is in this case given by (e.g., Proussevitch et al., 1993)

$$\frac{\partial c_i}{\partial t} + v_r \frac{\partial c_i}{\partial r} = \frac{1}{r^2} \frac{\partial c_i}{\partial r} \left(D_i r^2 \frac{\partial c_i}{\partial r} \right), \qquad (3)$$

where r is bubble radius, c_i is the concentration of volatile species i (either H_2O or CO_2), $v_r = dR/dt$ is the radial growth rate at the melt-vapor interface ($r = R$), and D_i is diffusion

coefficient of volatile species *i*. The boundary conditions are given by $\left(\frac{\partial c_i}{\partial r}\right)_{r=S} = 0$ and $(c_i)_{r=R} = s_i(p_g, x_c)$ (Gonnermann and Houghton, 2012). Here s_i is solubility of species *i* as formulated in Liu et al. (2005), p_g is the gas pressure within the bubble, and x_c is the mole fraction of CO_2 of the H_2O-CO_2 vapor mixture within the bubble.

We assume that each bubble grows in a closed system. Therefore, it follows that mass conservation is given by

$$\frac{d}{dt}\left(\rho_g R^3\right) = 4R^2 \rho_m \sum_i q_i \ , \qquad (4)$$

where ρ_m is melt density, and ρ_g is the density of the H_2O-CO_2 vapor mixture calculated from and equation of state (Kerrick and Jacobs, 1981). q_i is the diffusive mass flux of volatile species *i* and is calculated from the boundary condition $q_i = D_i\left(\frac{\partial c_i}{\partial r}\right)_{r=R}$.

The momentum balance is given by

$$p_g(t) - p_m(t) = \frac{2\sigma}{R} + 4\eta_e \frac{1}{R}\frac{dR}{dt} \ , \qquad (5)$$

where *t* denotes time, p_g is gas pressure inside the bubble, p_m is the pressure in the surrounding melt, σ is surface tension, η_e is effective viscosity of the melt (Lensky et al., 2001), which depends on the concentration of dissolved H_2O (Hui and Zhang, 2007).

Fragmentation and Permeability

The model calculations stop once the difference between pressure of the H_2O-CO_2 vapor mixture inside bubbles and the ambient pressure, $\Delta P = p_g - p_m$, exceeds the fragmentation threshold of Mueller et al. (2008)

$$\Delta P > \Delta P_f = (8.21\times10^5 \text{ MPa m}^{-1} \sqrt{k_1}\ \ 1.54 \text{ MPa}) / \phi. \qquad (6)$$

Here $\phi = R^3/S^3$ is the volume fraction of bubbles and the Darcian permeability, k_1, is calculated from ϕ using the formulation $k_1 = r^2(\phi - \phi_c)^n$ (e.g., Blower, 2001; Rust and Cashman, 2004; 2011) with values for ϕ_c, critical porosity, and *n*, power-law coefficient, as shown in Table 3 and corresponding to the curves shown in Fig. 3K.

CHARACTERISTIC TIME SCALE FOR PERMEABLE GAS FLOW

The characteristic time scale for pressure change by permeable gas flow, τ_k, is obtained from the equation for pore pressure diffusion (Wang, 2000), with the vapor phase approximated as an ideal gas (Kerrick and Jacobs, AJS, 1981), and the coefficient of storage approximated to first order by the inverse of gas pressure. The characteristic length scale, $L \sim 100$ m, is consistent with both the radial flow path, that is conduit radius, as well as the distance below fragmentation over which the magma attains significant permeability (Fig. 3).

REFERENCES CITED

Amon, M. and Denson, C.D., 1984, A study of the dynamics of foam growth: analysis of the growth of closely spaced spherical bubbles: Polymer Engineering Science, v. 24, p. 1026 – 1034.

Arefmanesh, A. and Advani, S., 1991, Diffusion- induced growth of a gas bubbles in a viscoelastic fluid: Rheology Acta, v. 30, p. 274 – 183.

Blower, J.D., 2001, Factors controlling permeability - porosity relationships in magma: Bulletin of Volcanology, V. 63, p. 497–504, doi: 10.1007/s004450100172.

Coombs, M.L. and Gardner, J.E., 2001, Shallow storage conditions for the rhyolite of the 1912 eruption at Novarupta, AlaskaL Geology, v.29, p. 775–778, doi: 10.1130/0091-7613(2001)029<0775:SSCFTR>2.0.CO;2.

Dobran, F., 1992, Non-eliquibrium flow in volcanic conduits and applications to the eruptions of Mount St. Helens, May 18, 1980 and Vesuvius in A.D. 79: Journal of Volcanology and Geothermal Research, v. 49, p. 285 – 311.

Forchheimer, P., 1900,Wasserbewegung durch Boden: Zeit. Ver. Deut. Ing., v. 45, p. 1781-1788.

Gonnermann, H.M. and Manga, M., 2007, The fluid mechanics inside a volcano: Annual Review of Fluid Mechanics, v. 39, p. 321–356, doi:10.1146/annurev.fluid.39.050905.110207.

Gonnermann, H.M. and Houghton, B.F., 2012, Magma degassing during the Plinian eruption of Novarupta, Alaska, 1912: Geochemistry, Geophysics, Geosystems, v. 13, p. 1 – 20.

Hammer, J.E., Rutherford, M.J. and Hildreth, W., 2002, Magma storage prior to the 1912 eruption at Novarupta, Alaska: Contributions to Mineralogy and Petrology, v. 144:, p. 144–162, doi:10.1007/s00410-002-0393-2.

Hildreth, W. and Fierstein, J., 2012, The Novarupta-Katmai eruption of 1912 - largest eruption of the twentieth century: centennial perspectives: U.S. Geological Survey, Professional Paper 1791.

Hui, H.J. and Zhang, Y.X., 2007, Toward the general viscosity equation for natural anhydrous and hydrous silicate melts: Geochimica and Cosmochimica Acta, v.71. p. 403 – 416.

Kerrick, D. M. and Jacobs, G.K., 1981, A modified Redlich-Kwong Equation for H_2O, CO_2, and H_2O-CO_2 mixtures at elevated pressures and temperatures, American Journal of Science, v. 281, p. 735–767.

Lensky, N., Lyakhoxsky, V. and Navon, O., 2001, Radial variations of melt viscosity around growing bubbles and gas overpressure in vesiculating magmas: Earth and Planetary Science Letters, v. 186, p. 1 – 6.

Liu, Y, Zhang, Y. X. and Behrens, H., 2005, Solubility of H_2O in rhyolitic melts at low pressures and a new empirical model for mixed H_2O-CO_2 solubility in rhyolitic melts: Journal of Volcanology and Geothermal Research, v. 109, B11203.

Mader, H.M., Llewellin, E.W. and Mueller, S.P., 2013, The rheology of two-phase magmas: A review and analysis: Journal of Volcanology and Geothermal Research, v. 257, p. 135–158.

Mastin, L. G., 2002, Insights into volcanic conduit flow from an open-source numerical model: Geochemistry, Geophysics, Geosystems, v. 3, no. 1037.

Moitra, P., Gonnermann, H.M., Houghton, B.F. and Giachetti, T., 2013, Relating vesicle shapes in pyroclasts to eruption styles: Bulletin of Volcanology, v. 75, no. 691, p. 1 – 14.

Pal, R., 2003, Rheological behavior of bubble-bearing magmas: Earth and Planetary Science Letters, v. 207, p. 165–179, doi: 10.1016/S0012-821X(02)01104-4.

Proussevitch, A., Sahagian, D. and Anderson, A., 1993, Dynamics of diffusive bubble growth in magmas: Isothermal case: Journal of Geophysical Research, v. 98, p. 22,283 – 22,307.

Proussevitch, A. and Sahagian, D., 2005, Bubble drive – 1: a numerical model of volcanic eruption mechanisms driven by disequilibrium magma degassing: Journal of Volcalonogy and Geothermal Research, v. 143, p. 89 – 111.

Reynolds, O., 1901, Papers on Mechanical and Physical Subjects: Cambridge University Press.

Rust, A.C. and Cashman, K.V., 2004, Permeability of vesicular silicic magma: Inertial and hysteresis effects: Earth Planetary Science Letters, v. 228, p. 93–107, doi:10.1016/j.epsl.2004.09.025.

Rust, A.C. and Cashman, K.V., 2011, Permeability controls on expansion and size distributions of pyroclasts: Journal of Geophysical Research, v. 116, p. 1–17, doi:0.1029/2011JB008494.

Wang, H.F., 2000, Theory of linear poroelasticity with applications to geomechanics and hydrogeology: Princeton University Press, Princeton, NJ, U.S.A., p. 1 – 287.

Wilson, L., Sparks, R.S.J. and Walker, G.P.L., 1980, Explosive volcanic erutions – IV. The control of magma properties and conduit geometry on eruption column behaviour: Geophysical Journal of the Royal Astronomical Society, v.63, p. 117 – 148.